REPORT R-555 APRIL, 1972 UILU-ENG 72-2216

CSL COORDINATED SCIENCE LABORATORY

ABSOLUTE INTENSITY MEASUREMENTS OF ELASTIC & INELASTIC LOW ENERGY ELECTRON DIFFRACTION FROM Al (100)

JAMES MICHAEL BURKSTRAND

UNIVERSITY OF ILLINOIS - URBANA, ILLINOIS

UILU-ENG 72-2216

ABSOLUTE INTENSITY MEASUREMENTS OF ELASTIC AND INELASTIC LOW ENERGY ELECTRON DIFFRACTION FROM Al (100)

by

J. M. Burkstrand

This work was supported in part by the Joint Services Electronics Program (U. S. Army, U. S. Navy and U. S. Air Force) under Contract DAAB-07-67-C-0199, in part by the American Chemical Society, Petroleum Research Fund under Contract PRF 3668-A3,5, and in part by the Air Force Office of Scientific Research, Office of Aerospace Research, USAF, under Grant AFOSR-71-2034.

This work is also being submitted to Physical Review for publication.

ABSOLUTE INTENSITY MEASUREMENTS OF ELASTIC AND INELASTIC LOW ENERGY ELECTRON DIFFRACTION FROM Al (100)*

J. M. Burkstrand†
Coordinated Science Laboratory and Department of Physics, University of Illinois, Urbana, Illinois 61801

ABSTRACT

Elastic and inelastic low energy electron diffraction (ELEED, ILEED) observations have been made on a clean surface of Al(100). Measurements on the (10) and (11) elastic diffraction beams were made using normally incident electrons in the energy range $30 \leq E \leq 170$ eV. Peaks in the energy loss distribution are seen near 5, 10, 15, 26 and 31 eV, the dominant peaks near 10 and 15 eV corresponding to surface and bulk plasmon excitations respectively. Two types of structure are observed in the inelastic angular profiles: one closely correlated with the structure in the elastic angular profile, and the second being substructure corresponding to different ILEED conditions. Energy intensity profiles (as a function of incident energy) for the (10) and (11) elastic and inelastic diffraction beams have been measured. These profiles also show primary and secondary structure. Within the substructure of the angular and energy intensity profiles are the first experimental observations of sideband diffraction. A comparison of the experimental results and the theoretical predictions of different models is made.

---

*This work was supported in part by the Joint Services Electronics Program (U.S. Army, U.S. Navy and U.S. Air Force) under Contract DAAB-07-67-C-0199, in part by the American Chemical Society, Petroleum Research Fund under Contract PRF 3668-A3,5, and in part by the Air Force Office of Scientific Research, Office of Aerospace Research, USAF, under Grant AFOSR-71-2034.

†Address as of 7/1/72: General Motors Research Laboratories, Department of Physics, Warren, Michigan 48090.

I. Introduction

In this paper we present a study of the electronic structure of Al(100) conducted by analyzing the differential inelastic cross sections of electrons in the energy range $0 \lesssim E \lesssim 300$ eV which have excited bulk and surface plasmons. In this energy range, the electrons' interactions with the metallic ion cores and valence electrons are so strong that they penetrate only a few atomic layers into the bulk. An analysis of their inelastic differential cross sections permits the determination of the dispersion relations for various electronic excitations in the metals and the nature of the coupling between the probe electron and the excitation.[1-4]

We report here the measurements of the absolute intensities of both the elastic and inelastic electrons diffracted into nonspecular directions. We then compare these measurements with the predictions of various models which describe elastic[5-11] and inelastic[1-4,12-14] low energy electron diffraction. It is not our objective to measure the plasmon dispersion relations from these results, but to check the consistency of the results with the models' predictions. It has been shown[8] that the large angle elastic scattering, such as seen in the nonspecular diffraction is more difficult to analyze than the smaller angle specular scattering. The uncertainty in the elastic scattering carries over to the analysis of the inelastic scattering and makes quantitative analysis difficult. However, it is still possible to extract from the data useful qualitative results, especially since the surface plasmon and bulk plasmon losses are easily identified in aluminum.

We shall demonstrate that the experimental measurements are consistent with the two-step model of inelastic low energy electron diffraction

(ILEED). In particular, a single-step model of the loss process is inadequate in describing the results. The phenomenon of sideband diffraction[12,13] is observed in the angular profiles of electrons which have excited bulk plasmons. Structure is seen in the inelastic energy intensity profile of these electrons which might also be due to sideband diffraction, although recent calculations[4] indicate that similar structure can be accounted for by multiple elastic scattering.

We proceed by briefly reviewing in section II the historical and theoretical foundation for this work. Section III is devoted to a description of the apparatus and the experimental procedure. It includes a discussion of the preparation and cleaning of the target surface, as well as a discussion of how the surface conditions are monitored.

We report in section IV our measurements of

$$\frac{d^2\sigma(E_p,w,\theta_s,\phi_s)}{d\Omega_s dE_s},$$

i.e., the elastic ($w = 0$) and inelastic ($w \geq 0$) differential scattering cross section for electrons incident in a normal direction on the target crystal. In this expression, E_p is the energy of the incident electrons, $E_p - w$ is the energy of the scattered electron, and θ_s, ϕ_s are the scattered polar and azmuthal angles respectively. We present absolute intensity measurements of the differential cross sections as a function of these parameters.

The experimental measurements are displayed in three forms: energy intensity profiles, energy loss profiles, and angular profiles. The energy intensity profiles are plots of the scattered intensity as a function

of the incident or primary energy E_p. The energy loss profiles are plots of the scattered intensity as a function of the energy loss w, and the angular profiles are graphs of the intensity as a function of the scattered polar angle or collector angle θ. In measuring the energy intensity profile of a nonspecular diffraction beam, we vary θ to follow the beam as it moves in space as a function of E_p. Except for this, the other parameters were held constant for each profile measurement. We selected ϕ_s to obtain the desired $\underset{\sim}{g} = (h,k)$ diffraction direction. A general discussion of the results is given in this section together with the experimental measurements.

Section V is devoted to a comparison of the experimental results with some theoretical predictions of both the elastic and inelastic profiles. It is found that the absolute intensities, both elastic[8] and inelastic[3,15] are predicted by an expanded version of the inelastic collision model. The two-step diffraction version of this model also predicts the main features of the inelastic cross-sections. Finally, in section VI, we give a summary of our results and the conclusions which we have drawn from them.

II. Theoretical Preliminaries

In 1927, Davisson and Germer[16] discovered that electrons can diffract coherently from a single crystal lattice. The phrase low energy electron diffraction (LEED) has been applied to this phenomenon involving electrons with energies in the range $15 \lesssim E \lesssim 300$ eV which have elastically scattered from the lattice. In this work, we denote the difference between the electrons which undergo elastic and inelastic low energy electron diffraction by ELEED and ILEED respectively. We include in ELEED those electrons

that have lost an amount of energy that is nonresolvable with our instrument, such as by phonon stimulation. There are currently several good reviews[17-20] that trace the historical development and uses of ELEED, so we do not pursue this topic here. Figure 1 shows a typical energy distribution for a monoenergetic beam of electrons scattered from a metal. The elastics are electrons that, within the experimental energy resolution of the analyzer, have scattered from the crystal with no apparent energy loss. The inelastics are electrons which have scattered from the crystal and in the process have lost a characteristic amount of energy. Any structure which is classified as inelastic is found with a nearly constant energy difference w from the elastic electrons at E_p, regardless of the value of E_p. We use the phrase "nearly constant" because any given loss mechanism may produce structure within a small region of w, the exact value of w depending on dynamical scattering effects. The true secondaries and Auger electrons are found at nearly constant secondary energies, regardless of the value of E_p. They were not studied as a part of this work.

In constructing a model of ILEED, it is necessary to know the loss mechanism that produced a certain structure in the inelastic energy region. Aluminum is one of the few materials in which the loss mechanism creating the primary structure in the inelastic loss profile is generally accepted to be excitation of bulk and surface plasmons. High energy electron transmission experiments[21,22], high energy back-scattering experiments[23] and optical reflectivity experiments[24] have been compared with theoretical predictions[25,26] with the conclusion that in Al, the infinite wavelength bulk plasmon occurs near 15eV and the surface plasmon near 10 eV.

Since the discovery of LEED, a number of experimental studies[16,27-34] have demonstrated the connection between ELEED and ILEED involving low energy losses ($1 \lesssim w \lesssim 30$ eV). These studies led to the identification of a two-step process of inelastic diffraction as the primary mechanism in which inelastically scattered electrons escape the crystal. In this process, the detected electron can undergo elastic scattering from the crystal lattice (diffraction) and inelastic scattering (creation of a plasmon, etc.) in either sequence. There have been several formal analyses[35-37] of ILEED using a quantum field theory. However, Duke and Laramore[12,13], having expanded upon the elastic theory of Duke and Tucker[5] and Duke, Anderson and Tucker[6] have developed the only detailed theoretical calculations of ILEED intensities using a quantum field theory approach. A basic ingredient in this theory is the systematic utilization of a set of "surface" conservation laws of energy and momentum parallel to the surface. Their initial calculations first were extended to provide detailed predictions of inelastic scattering from clean Al surfaces. Subsequently, Duke and Landman[4] extended the two-step analysis of Duke and Laramore[12,13] and of Duke and Bagchi[1-3] to include the effects of multiple elastic scattering. They concluded that these effects are important primarily in the energy profiles of the inelastically scattered electrons. Hence the detailed analysis of our data is confined to the loss and angular profiles.

Because of the magnitude of the works just referenced, we only summarize here the types of effects expected. We call a process in which the electron undergoes an elastic diffraction from the lattice followed by an inelastic collision, such as in plasmon creation, an EI (elastic-inelastic) process. The reverse process of an inelastic diffraction will be called an IE

process. In either process, the surface conservation laws of energy and momentum parallel to the surface are obeyed for each interaction (E or I), and, consequently between the incident and final electron states. If the electron scatters coherently from successive layers of the lattice, a resonance occurs which in lowest order pertubration theory is the familiar Bragg scattering. This manifests itself in the elastic energy intensity profile as a peak at an energy called a Bragg energy, E_{Bragg}.

We expect a peak in the energy intensity profile for loss energy w whenever the energy of the beam undergoing elastic diffraction equals E_{Bragg}, guaranteeing the conservation of total momentum at the elastic vertex. This condition will be met once for the EI process at $E_p \approx E_{Bragg}$ and once for the IE process at $E_p \approx E_{Bragg} + w$. These equations hold if the excitation momentum and energy are small compared to the incident electron momentum and energy, as is the case with the surface and bulk plasmons we will consider. Besides these maxima, Duke and Laramore[12,13] predicted a maximum in the scattered intensity to occur whenever the total crystal momentum is conserved, that is, when the sum of the incident electron momentum, final electron momentum, and excitation momentum equals a bulk reciprocal lattice vector. They refer to such maxima as sideband diffraction peaks. Their presence is expected to be observed in the angular profiles, possibly in the energy profiles and probably in the energy loss profiles of electrons which have excited bulk plasmons (or any bulk loss with wavevector $\vec{p}$ (w) $\neq$ 0). The detection of the phenomena is dependent on the electronic properties such as the loss dispersion relation and electron damping and on the experimental energy and the angular resolutions. Unfortunately, however, it cannot be distinguished clearly in the energy profiles from multiple elastic scattering effects[4].

Because of the localization of the surface plasmon wavevector along the surface, the angular profiles of electrons which have excited surface plasmons are expected to consist of a doublet structure. The experimental measurement of this doublet structure depends upon the relative probabilities of each excitation direction, upon the dispersion relation, electron damping, and the energy and angular resolutions. The angular profiles of the electrons which have excited bulk plasmons usually are expected to consist of only a single peak. However, in regions of sideband diffraction, Duke and Laramore predicted that this singlet would become a doublet, changing back to a singlet again as the incident electron energy was varied. For realistic values of the plasmon energy and momentum, this doublet is expected to occur for incident energies near $E_{Bragg} + w$.

III. Apparatus and Experimental Procedure

A medium resolution (~ .5 eV, 3.5^{o}) scanning LEED apparatus was originally designed and developed by F. M. Propst and T. L. Cooper[30]. We have modified it to improve the energy-angular operational characteristics and to incorporate an ion gun for sputter cleaning of surfaces.

The basic instrument, shown schematically in Figure 21, consists of a four grid retarding field energy analyzer with a collimated Faraday collector, electron gun, target assembly and electrostatic shielding. The target is rotatable through ~345^{o} about an axis normal to its surface. The collector is rotatable through an angle θ, $12^{o} \lesssim \theta \lesssim 90^{o}$, about an axis which is perpendicular to the axis of rotation of the target and which intersects the target surface, the incident beam direction and the axis of target rotation.

The angle θ is the angular distance between the electrons detected by the collector and incident beam (which is normal to the target surface). The combination of the two modes of rotation allow measurements to be made in any backscattered direction, and the retarding grid analyzer can measure an energy loss profile (or energy distribution) in any chosen direction. The instrument is enclosed in a field free region and is housed in an ultra-high vacuum chamber whose base pressure during experimental measurements is about 1×10^{-10} torr.

The target is an ultra-high-purity (99.999%) Al single crystal[38], 3.8 cm x .9 cm x .24 cm in size with a 2-56 clear hole drilled near the top to permit attachment to the Al holder. This hole was EDM spark-cut so that little or no mechanical damage was introduced into the experimental region. The crystal is held in place by clamping it against a slot in an Al block. This slot prevents the crystal from rotating in the holder about an axis perpendicular to the face of the holder. The block, clamp, and screw are made of ultra-high-purity aluminum to prevent impurities from migrating to the target during annealing. This assembled block is bolted to the remaining target assembly and is aligned so that the incident electron beam impinges normally on the crystal surface.

The crystal was spark cut to less than 2 degrees from the (100) face, and was mechanically polished flat to less than ten microns with silicon carbide grit. The surface was etched in a dilute solution of HF between different grits to remove any work hardened material. The crystal was then chemically polished[39] after which it was electropolished flat in a few minutes in a solution[39] of ethanol and perchloric acid. Polishing was carried out with

the bath temperature at about -15°C and at a current density of .1 to .15 amp/cm^2 and with constant, but mild, agitation. The perchloric acid polishing solution was chosen over others primarily because it is thought to leave[40] a relatively thin (~30 A°) oxide layer on the surface.

The crystal surface was cleaned using the method introduced for Al by Jona[41,42] and verified by others[40,43,44]. The target first was submitted to a bombardment of argon ions at 450 eV and about 3-5 μ amp/cm^2. This was followed by a vacuum anneal at 500°C for one hour. Five or six treatments consisting of bombardment followed by annealing produced a clean surface. The crystal was rotated at 6°/min during ion bombardment to assure uniform cleaning. Every third cycle, the annealing time was extended to two hours to assure that the damage introduced by the ion bombardment was annealed away.

We have used four basic tests of the cleanliness of our target surface. The least sensitive, but one which gives the order of magnitude of cleanliness and is most attainable, was the reproducibility of the ELEED pattern and the elastic energy profile. We also observed the Auger spectra of the surface after multiple cleanings and found no evidence of contaminents. However, the present apparatus was not designed to do high sensitivity Auger work (better than ~.1 monolayer sensitivity).

It is possible to monitor our surface cleanliness to coverages better than the ~.1 monolayer of O_2 coverage provided by the Auger measurements by using the technique of electron loss spectroscopy and the reproducibility of the surface plasmon loss profiles. It has been found both by us and by Edwards[45] that when O_2 is added to a clean surface of W, a new peak in the energy loss profiles may be measured near 7 eV. This author determined that

it is most easily found near energy and angular conditions of Bragg resonances, and its presence is detectable with about .05 monolayers of O_2 on the surface, using accepted values of the sticking probabilities. This loss peak was also measured on the Al surface in the presence of O_2. If we assume the same sensitivity as on W, we can say our surface is free of O_2 to less than .05 monolayers. The surface plasmon loss peak near 10 eV was also present during the measurements on Al.

The most sensitive test to change appears to be the reproducibility of the surface plasmon angular and loss profiles. Changes in the peak positions and intensities could be measured about 8 hours after argon bombardment and annealing, or with about .02 to .03 monolayer coverage of background (mostly H_2) gas, or $\lesssim$ .01 monolayer of O_2, (using the values of the sticking coefficients as determined by Jona[41] and Marsh[40].)

All our measurements reported here as being taken on a clean surface of Al were taken within 5-6 hours after each sputter-anneal cycle and in a background pressure of ~1-2 x 10^{-10} Torr. Thus, we expect no more than .01 to .05 monolayer of adsorbate on the surface during our clean measurements.

IV. Experimental Results and Discussion

This section is devoted to the presentation of the experimental measurements and a general discussion of the results, whereas the following one is devoted to a detailed comparison of the theoretical profiles and experimental measurements. The profiles will be presented in a set of normalized units, so that the diffracted beam intensities can be compared with each other and with the intensity of the incident beam. The method for making these comparisons, the first of their kind for inelastically diffracted electrons,

together with an intensity analysis is given in the first subsection. The subsequent three subsections are devoted to the presentation of the energy, loss, and angular profiles respectively.

A. Measurement of the Absolute Intensity

The object of our measurements was to determine the percentage of electrons scattered into a particular region of the energy-angle space, and then use this as a calibration for the rest of the measurements. To accomplish this, we must: (1) measure the total electron current incident on the target, (2) measure the electron current scattered into a particular beam in the desired energy-angle space, and (3) compare the experimental measurement (detector output) of this beam profile with the scattered percentage of incident current to get a conversion factor for the electronic output.

Figure 3 shows the measurements made in a calibration experiment to determine the desired conversion factor. In this calibration run, the incident electron current to the target, I_o, was measured at 5.0×10^{-6} amperes, which is the sum of the target current and the current to the electronic shielding. Since the electron gun is the only source of electrons, and since the current is conserved, this measurement gives the total incident current. We next took an angular profile of the elastically scattered electrons, as shown in Figure 21 (b). To measure the currents, we located our collector at 34^{o}, to correspond to the peak in the elastic angular profile. We then measured the retarding energy curve and the energy loss profile, as shown in the other two panels. For a collector of energy acceptance width approximately equal to the incident electron beam width, about 1 eV in our case, the total

scattered elastic current is approximately the current at a loss energy equal to the energy width. In these measurements we found I (Elastic) = $.1 \times 10^{-8}$ A.

The measured height of dI/dE for the elastic beam is .76 units; these units are applicable when the values of all variables such as amplifier gain, etc., set in the calibration experiment are used. Then an experimental height of .76 units corresponds to a percentage reflection equal to $.1 \times 10^{-8}/5 \times 10^{-6}$ or .02% I_o. Thus, one unit equals approximately .026% I_o. This factor has been applied to all the measurements, with proper account being taken for amplifier gain, etc. To make the measurements easier, we convert the scale to "normalized units", in which one normalized unit equals .01% I_o. If a curve has been amplifier for clarity, this will be denoted on the profile as a gain in parenthesis after the fixed variable, such as E_p = 100eV(x10), indicating that the particular profile is for a primary energy of 100 eV and is shown amplified by a factor of 10. For convenience, we have also included the amplification factor on the intensity scale shown on the experimental profiles. Thus the absolute intensity of each curve can be read directly from the graphs.

B. Energy Intensity Profiles

This subsection is devoted to the discussion of the experimental measurements of the elastic and inelastic energy intensity profiles. The profiles discussed are those of the (10) and (11) diffraction beams resulting from the diffraction of electrons incident normally on a clean surface of Al(100). In obtaining the energy intensity profiles, a series of angular

profiles was taken over the range of incident electron energies for each desired loss energy. The intensity was then measured at the desired collector angle by subtracting the extrapolated incoherent background and normalizing to unit incident beam current. The inelastic intensity for each incident energy was measured at the collector angle at which the elastic angular profile at that incident energy was a maximum, called $\theta_{Elastic}$. Figures 4 and 5 show the measured elastic (w = 0) and inelastic (w = 8 - 18 eV) energy intensity profiles for the (10) and (11) diffraction beams respectively.

1. Elastic Energy Intensity Profiles

The (10) elastic energy intensity profile has two major peaks at 54 and 107 eV. The (11) profile has three major peaks at 43, 86 and 152 eV. The major peaks in each profile are distinct, well separated in energy, and of halfwidth 10-12 eV. These peaks correspond to kinematical Bragg peaks resulting from a single scattering if an inner potential correction of about 14 eV is used. This is most easily seen by comparing our experimental peak locations with those predicted theoretically by Laramore and Duke[8] and found in Table 1. The inner potential of 14 eV locates all of our experimental peaks within 1 eV except for one which is within 2 eV.

We can also compare our elastic measurements with those of Jona[42] and Farrell and Somorjai[46]. Their experimentally determined peak locations are also found in Table 1. For the most part, the agreement with the work of Jona is good, while that with Farrell and Somorjai is adequate.

There are two low energy peaks in the (10) beam profile at 33 and 40 eV. The (11) profile shows two peaks at 54 and 63.5 eV and some less

prominent peaks at 112, 121, and 130 eV. Jona's profiles show these secondary peaks near 34 and 42 eV in the (10) profile and at 68 and 120 eV in the (11) profile. These are probably multiple scattering resonances, as we see in section V.

2. Inelastic Energy Intensity Profiles

An examination of the inelastic intensity profiles for both diffraction beams, Figures 4 and 5, shows that the structure for each loss energy is closely correlated with the structure in the corresponding elastic profile. For example, the gross structure in the inelastic profile occurs at about the same energies as the structure in the elastic profile. The dotted region of the profiles was that region in which the inelastic diffraction beams were not defined well enough relative to the background to permit an accurate measurement of their intensity. The dotted line represents the estimated intensity in this region.

Confining our attention to the energy region around the major peaks in the elastic profile, we first note that a peak occurs in the inelastic profiles at about the energy that the elastic profile has a Bragg peak (within 1 eV). This inelastic peak at E_{Bragg} is principally associated with those electrons whose scattering amplitude for elastic diffraction followed by an inelastic scattering (EI) is large.

We also expect to see a peak in the inelastic profile for loss energy w at $E_{Bragg} + w$ which is principally associated with those electrons whose scattering amplitude for an inelastic scattering followed by elastic diffraction is large (IE scattering). Indeed, peaks are experimentally observed at $E_{Bragg} + w$ within $\pm$ 1 and 2 eV for a majority of

the inelastic energy profiles in both the (10) and (11) diffraction beams. The clearest example of this is seen around the (11) Bragg peak at 86 eV. For electron losses between 10 and 16 eV, we find a prominent peak at 86 eV, corresponding to EI scattering, and a second peak located above this which moves away in energy as the loss energy increases, corresponding to IE scattering.

However, for a loss energy of 18 eV, the inelastic profile around E_p = 86 eV has become a four peaked structure. As the electrons which have lost 18 eV are those which have primarily excited bulk plasmons, the presence of four peaks is an indication of possible sideband diffraction. Recent calculations by Duke and Landman[4] indicate that the four peaked structure in the inelastic energy profiles can also be an effect of multiple scattering. The phenomenon of sideband diffraction is evident, however, in the inelastic angular profiles.

C. Energy Loss Profiles

In this subsection, we survey the phenomena observed in the energy loss profiles.

Figure 6 shows a series of energy loss profiles. As discussed in section II, the prominent peak near w = 10 eV corresponds to the excitation of a surface plasmon, the peak near 15 eV to the excitation of a bulk plasmon. While not shown in this figure, we observed the presence of a loss peak at 26 eV and another at w = 31 eV. The 26 eV loss possibly corresponds to the excitation of both a bulk and a surface plasmon, while that at 31 eV is possibly that of two bulk excitations. Finally, we also observed a series of loss peaks between 4.0 and 6.0 eV, and one at 8.0 eV. Figure 6 shows three

energy loss profiles taken in the (10) diffraction direction at different collector angles. The peak in the angular distribution of the 56 eV elastic electrons occurred at a collector angle of 31^{o}. In it we see a loss peak at 4 eV, a shoulder at ~ 5.5 eV, and a shoulder at ~ 8.0 eV each occurring on a different profile. We suspect that the 4 to 6 eV losses are due to a single loss mechanism, such as an interband transition, and the 8 eV loss is due to a separate, but unknown loss mechanism.

Figure 7 shows a striking example of the types of changes in the loss profiles which are measured upon adsorption of some background gas amounting to about .35 to .5 monolayers (using the assumed sticking probabilities and pressure measurements). The loss peak at 11 eV has decreased in intensity and shifted to 10 eV with the addition of gas on the surface. This absorption is in general agreement with the predictions of the theory[26] and experiments[23] done on Al films. The loss profile of the clean Al surface could be reproduced by argon bombardment and annealing of the "dirty" surface. One of the problems of using this type of criteria for a measure of surface cleanliness is that the surface plasmon losses from different primary beam energies and in different directions reacted with different degrees of sensitivity to the same contamination. We are now in the process of investigating the behavior of the surface plasmon dispersion relation as a function of gas coverage, which will be published in the near future as a separate work.

Finally we examine the effects of different diffraction conditions on the energy loss profiles. Figure 8 shows a series of energy loss profiles taken at different primary energies (E_p = 80 - 100 eV) and at three different relative collector angles. We have defined $\theta_{Elastic}$ as the angle at which the

elastic angular profile is a maximum. In other words, it is the angle relative to the surface normal at which the wavevector of the diffracted electron intersects the reciprocal lattice rod in an Ewald construction. We have chosen the various primary energies so as to encompass the (11) Bragg energy at 86 eV. Recalling Figure 5, we see that this choice of primary energies moves from a range primarily of EI diffraction to a range primarily of IE diffraction.

The most obvious feature evident in the figure is the relative growth and decay of the surface and bulk plasmons as a function of primary energy and scattering angle. First, for the collector angles constant with respect to $\theta_{Elastic}$, we note that for primary energies below the Bragg energy, there is a large surface plasmon loss peak at w = 10 eV and only a shoulder of a bulk plasmon loss. As the incident energy increases through the Bragg energy, the bulk plasmon loss grows relative to the surface plasmon until at E_p = 100 eV, there is a large bulk plasmon loss peak at w = 15 eV and only a shoulder of a surface plasmon loss. The rate of increase and decrease is dependent on the angle relative to $\theta_{Elastic}$, as can easily be seen by comparing the three panels. This also is evident upon comparing the profiles for a constant incident energy, for example, those of E_p = 95 eV. For a collector angle less than $\theta_{Elastic}$, the loss profile consists of a large surface plasmon loss and a shoulder of a bulk plasmon loss. As the angle is moved to angles greater than $\theta_{Elastic}$, the loss profile consists of a large bulk plasmon loss and a shoulder of a surface plasmon loss.

Examination of the loss profiles also shows that the position of the peaks are a function of the primary energy. For instance, at $\theta_{Elastic}$, the surface plasmon loss peak is at 10 eV for E_p = 80 eV and at about 11 eV

for E_p = 95 eV. One can ask whether this shift is a real change as a function of different diffraction conditions, or whether it is an apparent change caused by the addition of a large bulk plasmon peak located near the surface plasmon. If we assume that the loss peaks are Gaussian curves with widths equal to the experimental widths (~ 2 eV) and separated by 5 eV then a numerical calculation shows that the addition of a second peak which is equal in height to the first will shift the first peak position by about .3 eV. Thus, the 1 eV experimental shift probably is a real shift which is a function of the incident electron energy. That this shift is real is further substantiated by comparison with the theoretical profiles in the next section in which it is seen to be a direct result of diffraction phenomena described by the two-step model of ILEED.

D. Angular Profiles

This subsection is devoted to an analysis of the measured angular profiles. Figure 9 shows a series of angular profiles at a constant primary energy (E_p = 92 eV). Note that the elastic profile (w = 0) is symmetrical and well localized in angle in what is commonly called a diffraction beam. If we examine the inelastic profiles ($w \neq 0$), we see that they too are found in localized beams which occur near the elastic beam. This is a consequence of inelastic two-step diffraction. Without a diffraction from the lattice, we would not expect to find the inelastics so well localized in angle. But there are dynamical scattering effects present, as can be seen in the internal structure of the inelastic profiles.

Figure 10 shows a series of angular profiles for losses of 10 and 12 eV respectively, taken at a number of different primary energies. The

range of primary energies includes values both above and below the (11) Bragg energy of 86 eV. The black dot on each profile indicates the position of the peak in the elastic angular profile for that particular incident energy. The behavior of these profiles is not exactly that expected of surface plasmon angular profiles if one considers a purely kinematic model of inelastic diffraction. This type of model, such as given by the Ewald collision diagram[18] predicts a sharp double peaked structure in the inelastic angular profiles for all incident energies. Even a quantum field theoretical treatment (QFT)[13] predicts a doublet structure at all energies. However, as described in the next section, the QFT treatment also predicts that large intensity differences can occur between the two peaks. Large internal damping effects, such as through decreased plasmon lifetimes, can then make these two peaks appear as a single peak. If the surface plasmons in question have a small wavevector, the finite angular resolution can make even two peaks of equal intensity appear as a singlet. It should be emphasized that the doublet structure <u>is</u> seen over a range of primary energies for the surface plasmon angular profiles.

Figure 11 shows a series of angular profiles for the 14 and 16 eV losses which were taken over a range of primary energies which includes the 86 eV Bragg energy. These profiles also are more or less localized around the elastic beam, indicating inelastic diffraction. As in the profiles of the surface plasmons, these angular profiles also display the motion of the inelastic peak from the low angle side to the high angle side of the elastic peak with increasing primary beam energy. The behavior of the diffraction substructure for the w = 16 eV loss profiles is an experimental verification of sideband diffraction. As the incident energy sweeps in value across the

Bragg energy, the profiles change precisely as predicted.[13] The profile begins as a singlet peak, which changes to a large doublet as the incident energy E_p increases. The high angle peak decreases in size relative to the low angle one until at some $E_p < (E_{Bragg} + w)$, there is only a singlet peak remaining. The singlet then splits into a doublet for larger energy, and as the incident energy is increased further, the profile returns to a small singlet.

However, the presence of a doublet peak is not necessarily evidence of sideband diffraction. Certain structure can be associated with a surface plasmon loss and hence the cause of an apparent splitting. For instance, if we examine Figure 9, we can observe the surface plasmon peak beginning at 10 eV move to slightly lower angles as we increase the loss energy to 13 eV. As we increase the loss energy to 17 eV the surface plasmon peak moves out more rapidly to lower angles, a consequence of the increasing plasmon wave-vector. But at the same time we see another peak just to the low angle side of the elastic peak grow for w = 14 and 15 eV. This peak, together with the peak on the high angle side is a bulk plasmon peak.

Thus, reexamining Figure 11 the doublet for E_p = 90 and 92 eV in the w = 16 profiles consists of a surface plasmon peak on the low angle side of the elastic peak and a bulk plasmon on the high angle side. However the doublet at E_p = 98 eV and again at E_p = 106 eV is a bulk plasmon doublet due to sideband diffraction. We arrive at the same conclusions by careful examination of the energy loss profiles at different collector angles.

As mentioned before, we expect that the profiles of the 14 eV loss will contain structure due to excitations of both the bulk and surface plasmons.

Figure 11 shows a series of angular profiles of electrons which lost 14 eV to the solid. The general behavior is similar to the profiles of the other losses: that of a singlet peak on the low angle side of the elastic peak changing to multiple peaks, and ending as a singlet peak on the high angle side of the elastic peak as the incident electron energy is increased to values greater than the Bragg energy.

The presence of these multiple peaks make the w = 14 eV angular profiles interesting. Figure 12 shows four of these profiles in more detail. The angular profile resulting from a bombardment of electrons with E_p = 90 eV clearly shows three peaks, with E_p = 92 eV two peaks with a hint of a third, and with E_p = 96 and 98 eV only two peaks. The two peaks which are on either side of the elastic peak by about 1^o - 1.5^o are a result of sideband diffraction of the bulk plasmon loss. The angular splitting is smaller than that seen in the 16 and 18 eV loss angular profiles because the wavevector of the excitation is smaller. The third peak is located 7^o to the low angle side of the elastic peak. Using the law of conservation of momentum parallel to the surface, a straightforward calculation leads to the result that the excitation's momentum parallel to the surface is about .6 Å^{-1}. As we see in the next section, this value is far too big for a bulk plasmon near this energy loss, but is about correct for a surface plasmon. We can make another analysis which, although qualitative, leads to the same conclusion. If we reexamine Figure 8, we see that for E_p = 90 eV and $\theta < \theta_{Elastic}$, the energy loss profile indicates that the 14 eV loss has a stronger surface plasmon component than bulk plasmon. However, for $\theta \gtrsim \theta_{Elastic}$, the bulk plasmon component dominates at w = 14 eV, which is what we just concluded from the angular profiles.

In addition to identifying the dynamical origin of various details in the measured intensities, we also can determine the dispersion relations of the surface and bulk plasmons from plots such as shown in Figure 9. We can do this by either making a straightforward kinematic calculation, using the law of conservation of momentum parallel to the surface, as done in a preceeding paragraph, or we can use a quantum field theoretical treatment as done by Duke and Bagchi[1-3]. The QFT treatment should yield a more accurate dispersion relation, because it takes account of the various dynamical scattering factors present. We refer the interested reader to references 1-3 for details of the calculation.

V. Comparison of Experimental and Theoretical Profiles

In this section, we compare some of our experimental profiles with some theoretical profiles calculated by Duke and Bagchi[1-3], Laramore and Duke[8], Hoffstein and Boudreaux[9], Jepsen, Marcus and Jona,[10] and Hirabayashi[11]. The profiles calculated by Duke and Bagchi are those describing the inelastic scattering intensities. The profiles calculated by the other authors are those describing the absolute elastic scattering intensities. It should be noted that Jepsen et al[10] calculated other elastic intensity profiles to fit the position and shapes of the experimental curves, but not for absolute intensity comparison.

There are substantial differences in the models used in these two sets of theoretical calculations. Laramore and Duke used a finite temperature version of the inelastic collision model[5,6] with an electron-ion-core potential described by s, p, and d partial wave phase shifts to describe the elastic

scattering from the solid. Bagchi and Duke, on the other hand, used an isotropic scattering version (s-wave scattering only) of the inelastic collision model which was also temperature independent in order to calculate a series of inelastic profiles. The less complete latter model was used only for those calculations of the angular and loss profiles for which they have been shown to be adequate[4].

Jepsen, Marcus and Jona's calculations were carried out using a method referred to as the layer-KKR method[47], which combines a treatment of multiple scattering in each layer by the Korringa-Kohn-Rostoker method of band theory with a propagation matrix method of handling multiple scattering between layers in a beam representation. Their calculations for the absolute reflected intensities did not consider inelastic damping, as they used a real potential in the scattering.

Hoffstein and Boudreaux used a band-structure-matching approach with no inelastic damping and with a pseudopotential based on the orthogonalized-plane-wave (OPW) approximation without any adjustable parameters. Finally, Hirabayashi used a "simplified" version of the s-wave inelastic collision model with no temperature dependence.

The results of three of the authors are shown in Figure 13, together with the measured experimental profiles. The results of Hoffstein and Boudreaux were qualitatively similar to those of Jepsen et al. As is readily seen, the best agreement between experiment and theory is found with the profiles calculated by Laramore and Duke. We will now compare the two in more detail.

The theoretical and measured line shapes of both the (10) and (11) beams agree well. The major peaks are in about the same places (refer to Table 1) and the secondary structure also is reproduced. See, e.g., the multiple scattering peak at about 62 eV in the (11) profile. The profiles differ in that the experimental peaks are about half as wide as the theoretical peaks.

The absolute intensities of the calculated and observed peaks are found to be in quantitative agreement. The absolute intensity of the (11) Bragg peak at 86 eV was calculated to be .055% I_o and was measured to be .056% I_o, where I_o is the intensity of the incident electron beam. The agreement between the other (11) peaks is equally good. The absolute intensity of the (10) Bragg peak at 54 eV was calculated to be about .090% I_o and was measured to be .044% I_o, a difference of about a factor of 2. This difference can be rationalized by assuming a larger misalignment in this direction than in the (11) direction. This can occur as a consequence of rotating the target to bring the (10) diffraction plane into the plane of the collector rotation (see reference 30 for details). In general, the agreement between the calculated and observed intensities is surprisingly good with regard to the absolute magnitude as well as the line shape of both the elastic and inelastic intensities. Although the models used by Laramore and Duke in the calculations are simplified, they seem to describe the scattering phenomena quite adequately.

Finally, we will look at a set of inelastic profiles calculated by Duke and Bagchi. First, with regard to the absolute magnitudes, when the experimental and theoretical elastic and inelastic energy intensity profiles are compared, it is found that the theoretical profiles are larger than the

experimental profiles (after normalization) by a factor of less than two. Thus the empirical electron-plasmon vertex used by Duke and Bagchi does, in fact, give approximately the correct relative intensities of the elastic and inelastic cross sections. Second, concerning diffraction phenomena predicted by the two-step model, Figure 14 shows a series of experimental and theoretical energy loss profiles, equivalent to the conditions described for Figure 8. As the primary energy increases above the Bragg energy at 86 eV, the strength of the bulk plasmon loss peak grows relative to that of the surface plasmon. This is seen in both the experimental and theoretical curves. Differences in relative intensities of the two losses can be explained by remembering that the experimental profiles contain the electrons which have scattered both coherently and incoherently from the solid, as well as electrons which have excited particle-hole excitations.

Figure 15 shows a set of theoretical and experimental angular profiles for w = 14 eV. The theoretical profiles were calculated with a set of parameters for illustrative purposes only. The theoretical profiles show the two surface plasmon peaks on the very low and very high angle sides of $\theta_{Elastic}$, together with a bulk plasmon loss. The bulk plasmon is first seen as a singlet on the low angle side of $\theta_{Elastic}$ at E_p = 84 eV, after which it becomes a doublet about $\theta_{Elastic}$ for E_p = 88 and 90 eV. For larger values of E_p, the peak gradually becomes a single peak located on the high angle side of $\theta_{Elastic}$. This is the behavior we see in the experimental profiles (also refer back to Figures 11 and 12). As was pointed out in Figure 12, we clearly see the low angle surface plasmon and the two bulk plasmon peaks due to sideband diffraction at E_p = 90 eV, together with the motion of the peak across $\theta_{Elastic}$.

VI. Summary of Results and Conclusions

The data presented in the previous two sections demonstrated clearly the existence of inelastic low energy electron diffraction. At the same time, the two-step model of ILEED was verified, by virtue of our reporting two peaks in the inelastic energy intensity profiles representing EI and IE diffraction, and measuring the predicted[1,3] systematic correlations between the elastic and inelastic angular profiles based upon this model.

Examining the inelastic profiles in detail, we established the dependence of inelastic diffraction on different diffraction conditions. The energy loss profiles demonstrated a new behavior in the change in the relative heights of the surface and bulk plasmon losses as the primary energy is swept across a Bragg energy. This provides a new test in distinguishing between the two types of losses in materials where the losses are not clearly known. We also observed the predicted doublet structure in the surface plasmon angular profiles which is due to the localization of the excitation momentum along the surface. We reported for the first time the experimental observation of sideband diffraction for a bulk plasmon excitation. We observed the predicted sideband diffraction in the inelastic angular profile and possibly in the inelastic energy profile.

The energy loss profiles indicate the occurrence of some low energy losses whose presence is detected only under certain energy and momentum conditions. A high resolution energy-angular instrument probably would yield information on the nature of these losses. We also demonstrated that ILEED is sensitive to surface conditions.

The comparison of the experimental and theoretical profiles indicates that the inelastic collision model yeilds an adequate description of low energy electron diffraction. The experimental profiles, when coupled with this model of inelastic diffraction, yield[1-3] an adequate description of the plasmon dispersion relations, coupling relations, damping parameters, etc., thus increasing our knowledge of the chemical and electronic properties of solid surfaces.

ACKNOWLEDGEMENTS

The author is indebted to: Professor C. B. Duke, Dr. G. E. Laramore, Dr. A. Bagchi, and Dr. U. Landman for many invaluable discussions concerning the theory of inelastic diffraction and for copies of their results pertaining to our experiment prior to publication; to Professor F. M. Propst for his helpful experimental contributions during the course of this work; to Dr. T. L. Cooper for designing and constructing the original instrument; to Professor M. Metzger, for supplying the aluminum crystal and his technical experience in its preparation; and to the technical staff of the Coordinated Science Laboratory for their enthusiastic and imaginative technical assistance in their respective fields.

REFERENCES

1. C. B. Duke and A. Bagchi, Program of the 1971 International Conference on Solid Surfaces, J. Vac. Sci. Technol. 9, ...(1972).

2. A. Bagchi, et al., Phys. Rev. Letters 25, 998 (1971).

3. A. Bagchi and C. B. Duke, Phys. Rev. B5, (1972); ...(private communication).

4. C. B. Duke and U. Landman, (to be published).

5. C. B. Duke and C. W. Tucker, Jr., Surface Science 15, 231 (1969).

6. C. B. Duke, J. R. Anderson and C. W. Tucker, Jr., Surface Science 19, 117 (1970).

7. C. B. Duke et al., Surface Science 27, 523 (1971).

8. G. E. Laramore and C. B. Duke, Phys. Rev. B5, 267 (1972).

9. V. Hoffstein and D. S. Boudreaux, Phys. Rev. Letters 25, 512 (1970).

10. D. W. Jepsen, P. M. Marcus and F. Jona, IBM Research Report RC3525 (#15956), (1971).

11. K. Kirabayashi, Surface Science 28, 621 (1971).

12. C. B. Duke, G. E. Laramore, and V. Metze, Solid State Commun. 8, 1189, (1970).

13. (a) C. B. Duke and G. E. Laramore, Phys. Rev. B3, 3183 (1971).

    (b) G. E. Laramore and C. B. Duke, ibid. 3198 (1971).

14. C. B. Duke, A. J. Howsmon and G. E. Laramore, J. Vac. Sci. Technol. 8, 10 (1971).

15. Corrections in the absolute intensity scales of references 3 and 8 have been made by U. Landman and C. B. Duke. Reference 3 was corrected by changing from scattering to reflection boundary conditions and by changing the strength of the bulk plasmons by a factor of two. Reference 8 was corrected by changing the normalization factor by a factor of about four.

16. C. Davisson and L. H. Germer, Phys. Rev. 30, 705 (1927).

17. J. W. May, Ind. Eng. Chem. 57, 18 (1965).

18. J. J. Lander, Prog. Solid State Chem. 2, 26 (1965).

References (continued)

19. P. J. Estrup and E. G. McRae, Surface Science 25, 1 (1971).

20. E. J. Scheibner and L. N. Tharp, Surface Science 8, 247 (1967).

21. Summarized by O. Klemperer and J. P. Shepherd, Adv. Physics 12, 355 (1963).

22. J. Swan, A. Otto and H. Gellenzer, Phys. Stat. Sol. 23, 171 (1967).

23. (a) C. Powell and J. Swan, Phys. Rev. 115, 869 (1959).

(b) C. Powell and J. Swan, Phys. Rev. 118, 640 (1960).

24. M. Williams, E. Arakawa and L. Emerson, Surface Science 6, 127 (1967).

25. R. H. Ritchie, Phys. Rev. 106, 874 (1957).

26. E. Stern and R. Ferrell, Phys. Rev. 120, 130 (1960).

27. P. P. Reichertz and H. E. Farnsworth, Phys. Rev. 75, 1902 (1949).

28. J. O. Porteus, in The Structure and Chemistry of Solid Surfaces, edited by G. A. Somorjai (Wiley, N.Y., 1969) p. 12-1.

29. M. P. Seah, Surface Science 17, 132 (1969).

30. T. L. Cooper, Ph.D. Thesis, University of Illinois, 1970; (to be published).

31. T. L. Cooper, J. M. Burkstrand and F. M. Propst, Program of the Thirtieth Annual Conference on Physical Electronics, 1970 (unpublished).

32. J. C. Turnbull and H. E. Farnsworth, Phys. Rev. 54, 507 (1938).

33. W. H. Weber and M. B. Webb, Phys. Rev. 177, 1103 (1969).

34. M. P. Seah, Surface Science 17, 161 (1969).

35. E. Bauer, Z. Physik 224, 19 (1969).

36. J. I. Gersten, Phys. Rev. 188, 774 (1969).

37. Y. H. Ohtsuki, J. Phys. Soc. Japan 29, 398 (1970).

38. The crystal was obtained from Professor M. Metzger, Dept. of Metallurgy and Mining, University of Illinois.

References (continued)

39. O. P. Arora and M. Metzger, Trans. Met. Soc. AIME, 236, 1205 (1966).

40. J. B. Marsh, General Electric Technical Information Series, No. 68-C-287 (1968).

41. F. Jona, J. Phys. Chem. Solids 28, 2155 (1967).

42. F. Jona, IBM J. Res. Develop. 14, 444 (1970).

43. W. D. Robertson, 1971 International Conference on Solid Surfaces, Boston, Mass.; (private communication).

44. D. T. Quinto and W. D. Robertson, Surface Science 27, 645 (1971).

45. D. E. Edwards, Ph.D. Thesis, University of Illinois, 1970; (to be published).

46. H. H. Farrell and G. A. Somorjai, Phys. Rev. 182, 751 (1969).

47. D. W. Jepsen and P. M. Marcus, Computational Methods in Band Theory (Plenum Press, N.Y., 1971), p. 416.

Table 1. Comparison between experimentally observed and theoretically predicated positions of the principal peaks (in eV) in the elastic elastic intensity profiles of the (11) and (10) diffraction beams from Al(100). V_I is the inner potential correction.

Experimental			Theoretical	
Jona[42]	Farrell and Somorjai[46]	This work	Laramore and Duke[8]	
			V_I=14	V_I=16.7
(11) beam:				
46		43	43	40
90	88	86	87	84
151	143	152	151	148
(10) beam:				
56	55	54	53	50
84	74	(75)	75	73
105	98	107	105	102

FIGURE CAPTIONS

Figure 1. Energy distribution of electrons scattered from a clean surface of Al(100).

Figure 2. Schematic of the energy-angular distribution instrument showing the basic components.

Figure 3. Experimental measurements necessary to calibrate the intensity of the scattered electrons.

Figure 4. Elastic and inelastic energy intensity profiles for the (10) diffraction beam. The intensity unit is labeled for each scale factor used.

Figure 5. Elastic and inelastic energy intensity profiles for the (11) diffraction beam.

Figure 6. Energy loss profiles for a primary energy of 56 eV and different collector angles. $\theta_{Elastic} = 31^{o}$.

Figure 7. Energy loss profiles in the (10) diffraction direction for a "clean" and "dirty" surface.

Figure 8. Series of energy loss profiles in the (11) diffraction beam for different primary energies, E_p, and collector angles θ.

Figure 9. Angular profiles for a constant primary energy (92 eV) and different loss energies.

Figure 10. Inelastic angular profiles for (a) w = 10 eV, (b) w = 12 eV, in the (11) diffraction direction. Each black dot indicates the position of the peak in the elastic angular profile for that particular incident energy.

Figure 11. Inelastic angular profiles for (a) w = 14 eV, (b) w = 16 eV, in the (11) diffraction direction. Each black dot indicates the position of the peak in the elastic angular profile for that particular incident energy.

Figure 12. Inelastic angular profiles, w = 14 eV, in the (11) direction. Each black dot indicates the position of $\theta_{Elastic}$ for each primary energy.

Figure 13. Theoretical, (a-c), and experimental, (d), elastic energy intensity profiles in the (11) and (10) diffraction directions. The theoretical profiles are by (a) Jepsen et al.[10], (b) Hirabayashi[11], and (c) Laramore and Duke[8].

Figure Captions (continued)

Figure 14. Theoretical and experimental energy loss profiles in the (11) diffraction direction. The theoretical profiles were calculated by Duke and Bagchi[1,3].

Figure 15. Theoretical and experimental inelastic angular profiles in the (11) diffraction direction for a loss energy of 14 eV. The theoretical profiles were calculated by Duke and Bagchi[1,3].

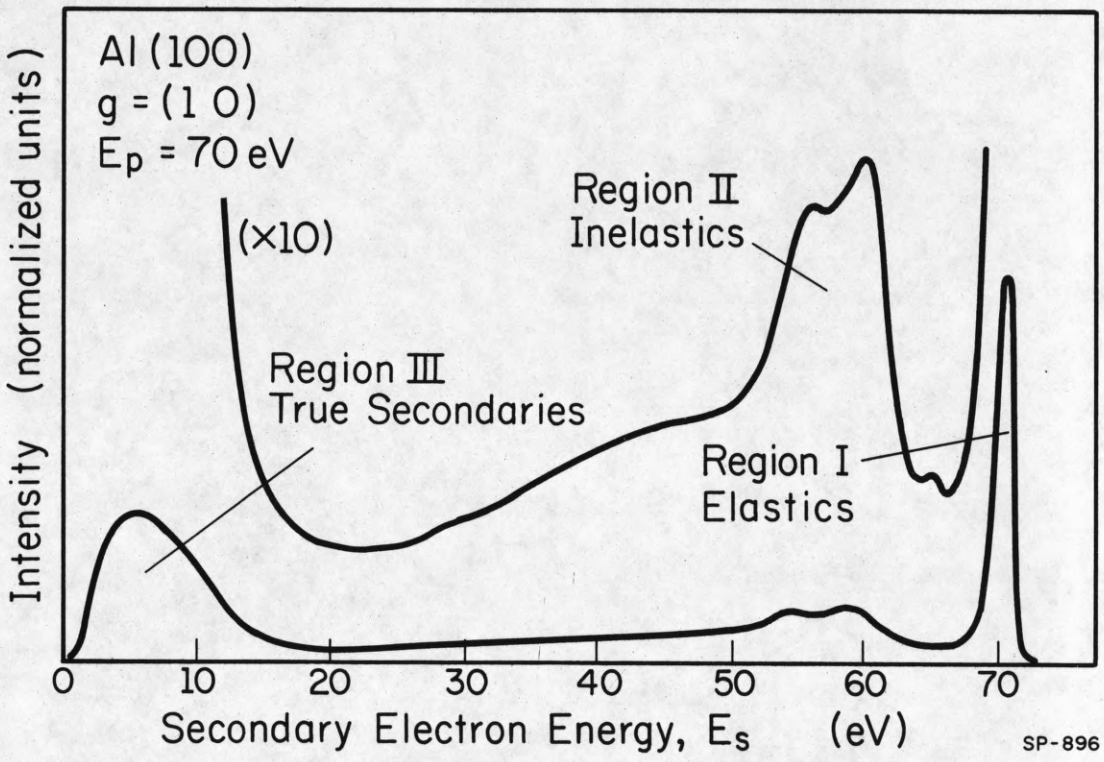

Figure 1. Energy distribution of electrons scattered from a clean surface of Al(100)

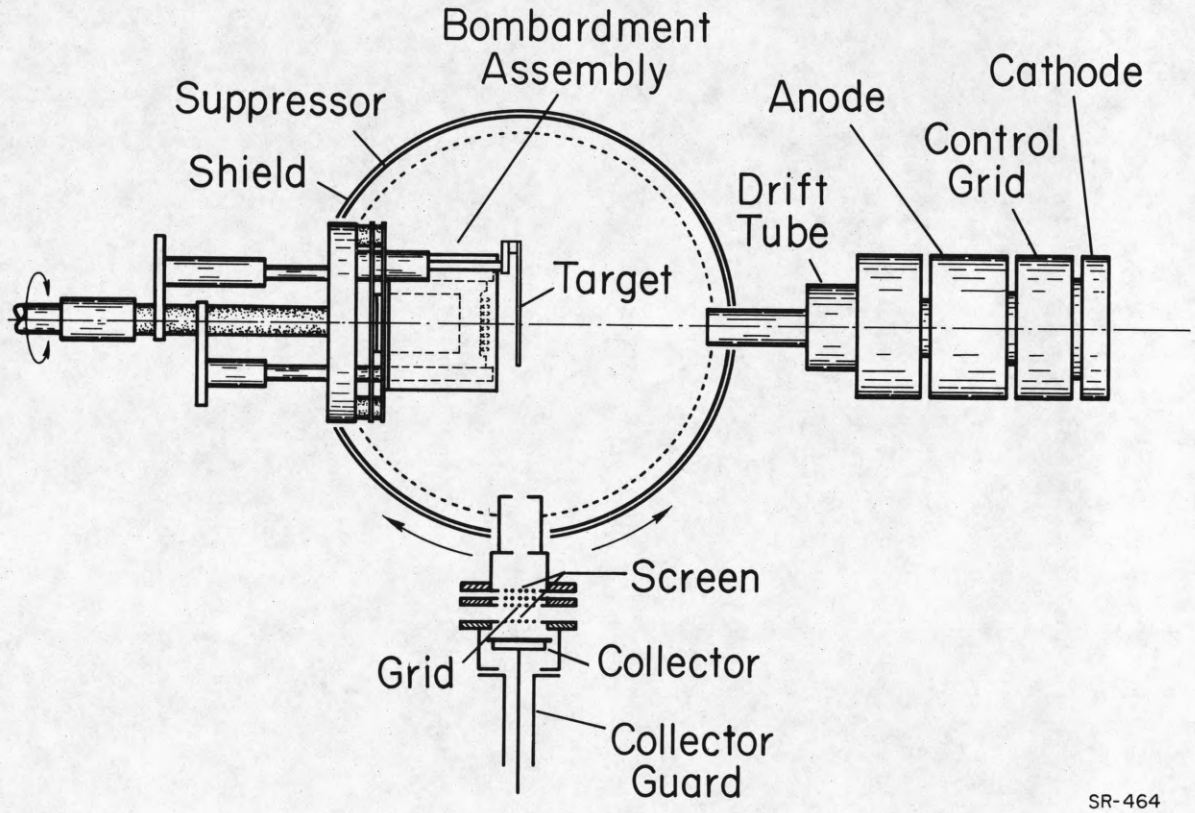

Figure 2. Schematic of the energy-angular distribution instrument showing the basic components

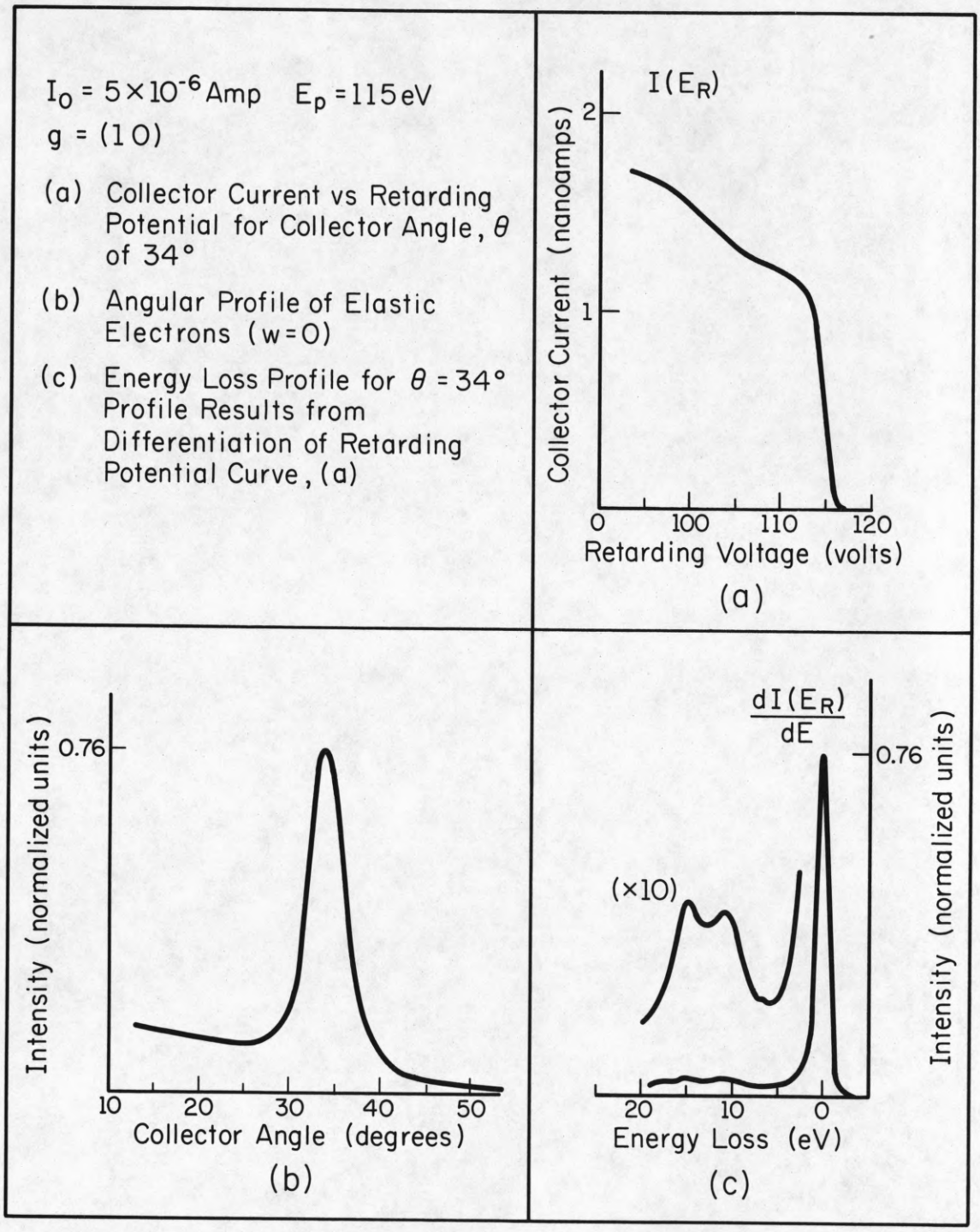

Figure 3. Experimental measurements necessary to calibrate the intensity of the scattered electrons

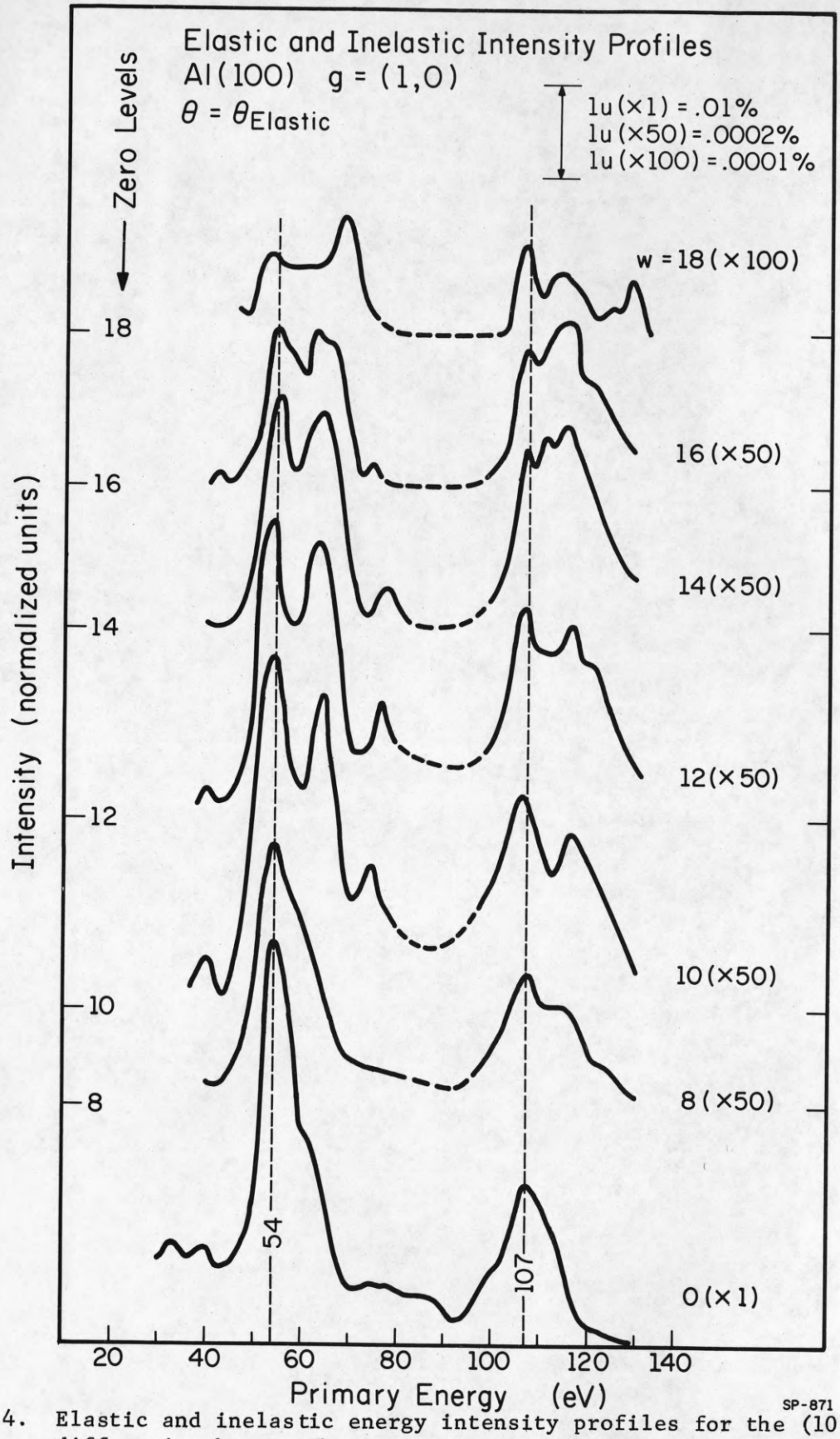

Figure 4. Elastic and inelastic energy intensity profiles for the (10) diffraction beam. The intensity unit is labeled for each scale factor used.

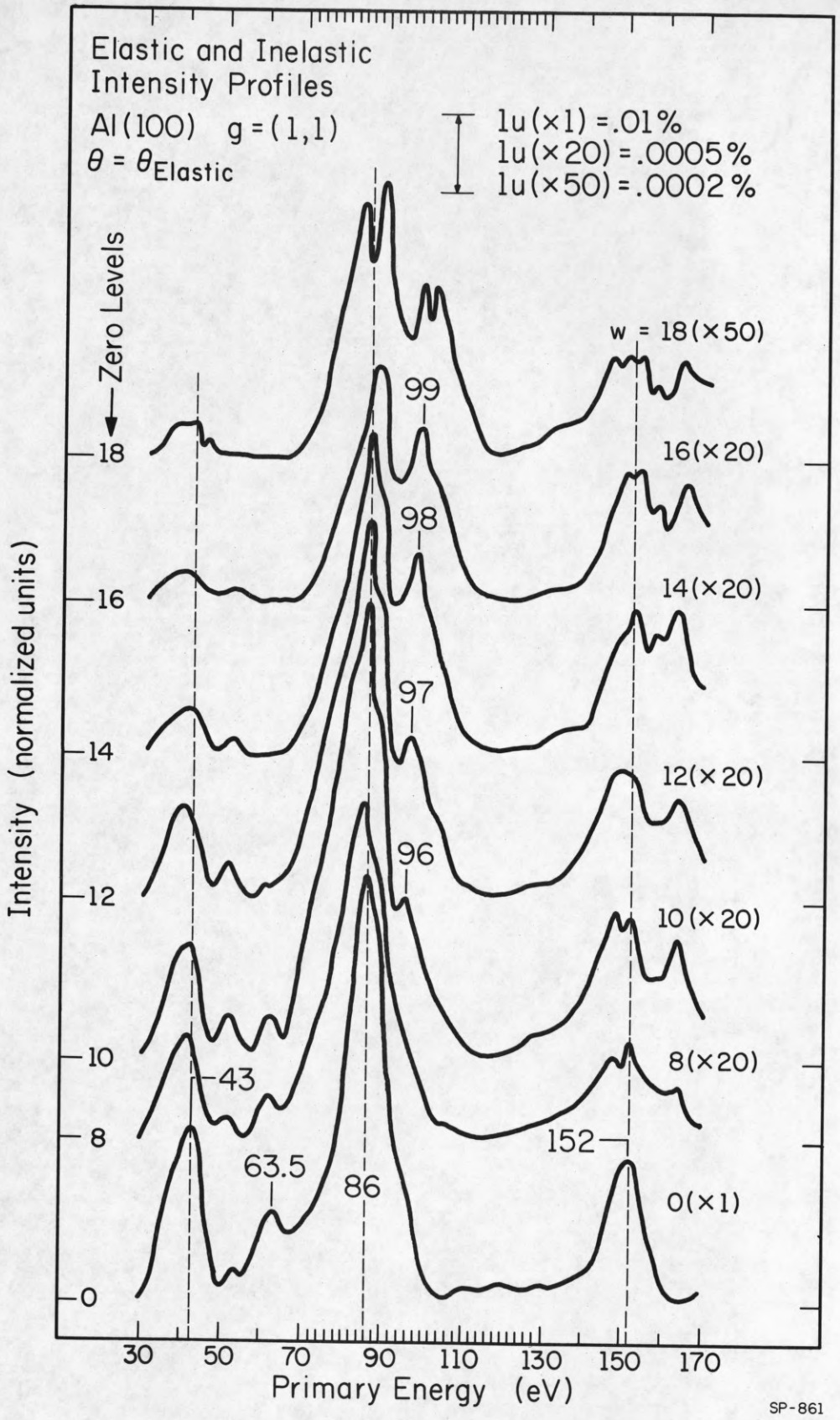

Figure 5. Elastic and inelastic energy intensity profiles for the (11) diffraction beam

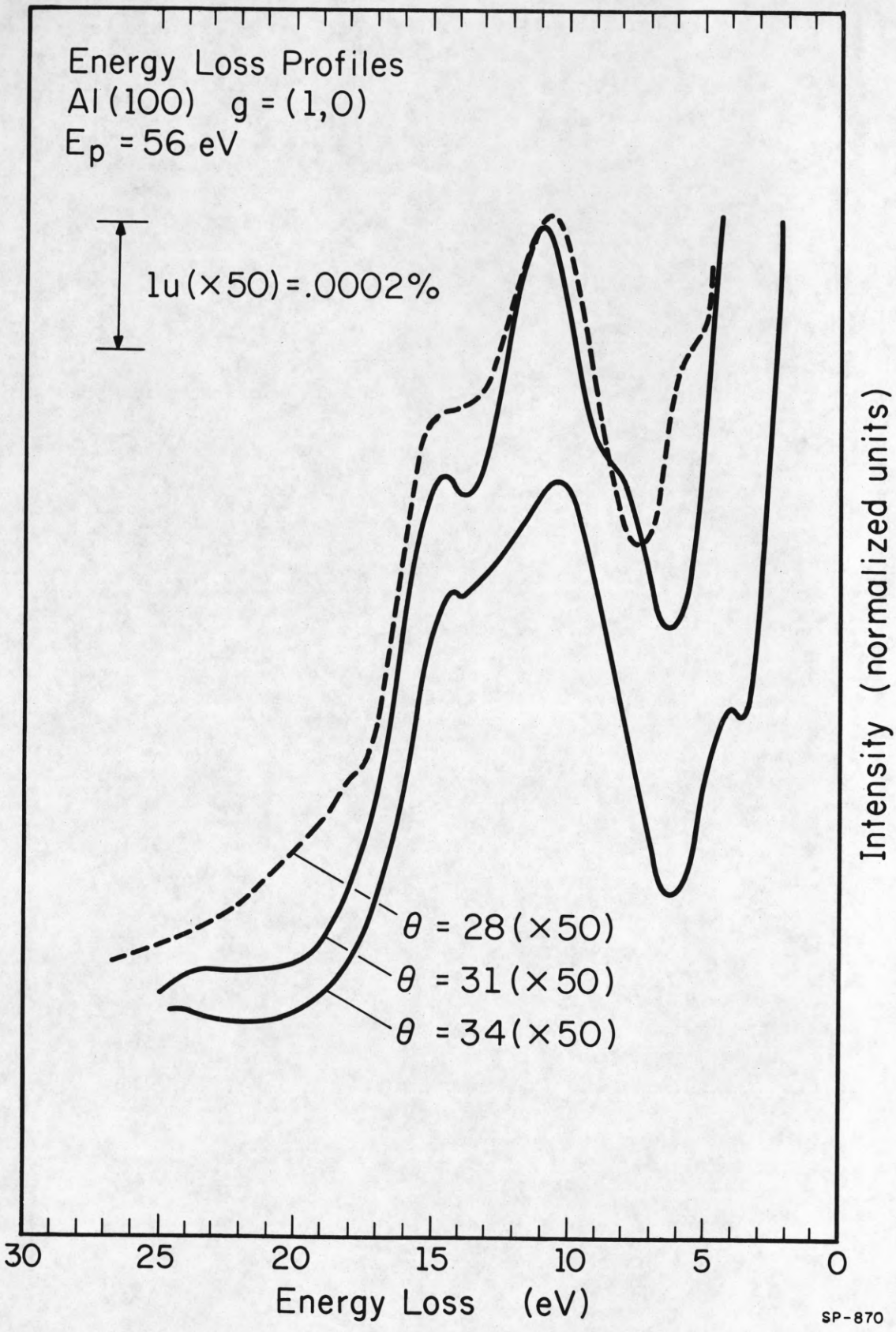

Figure 6. Energy loss profiles for a primary energy of 56 eV and different collector angles. $\theta_{Elastic} = 31^{o}$.

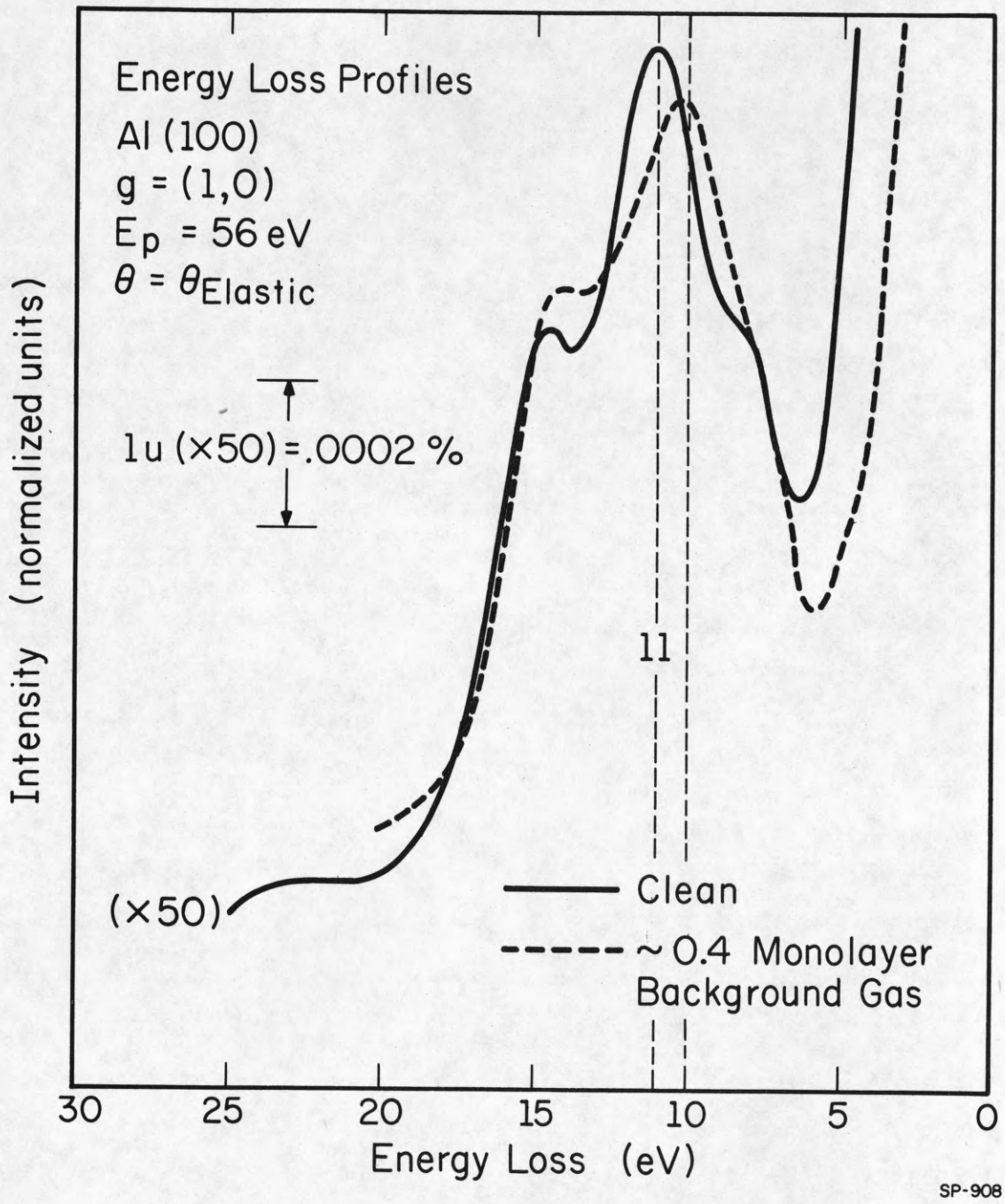

Figure 7. Energy loss profiles in the (10) diffraction direction for a "clean" and "dirty" surface.

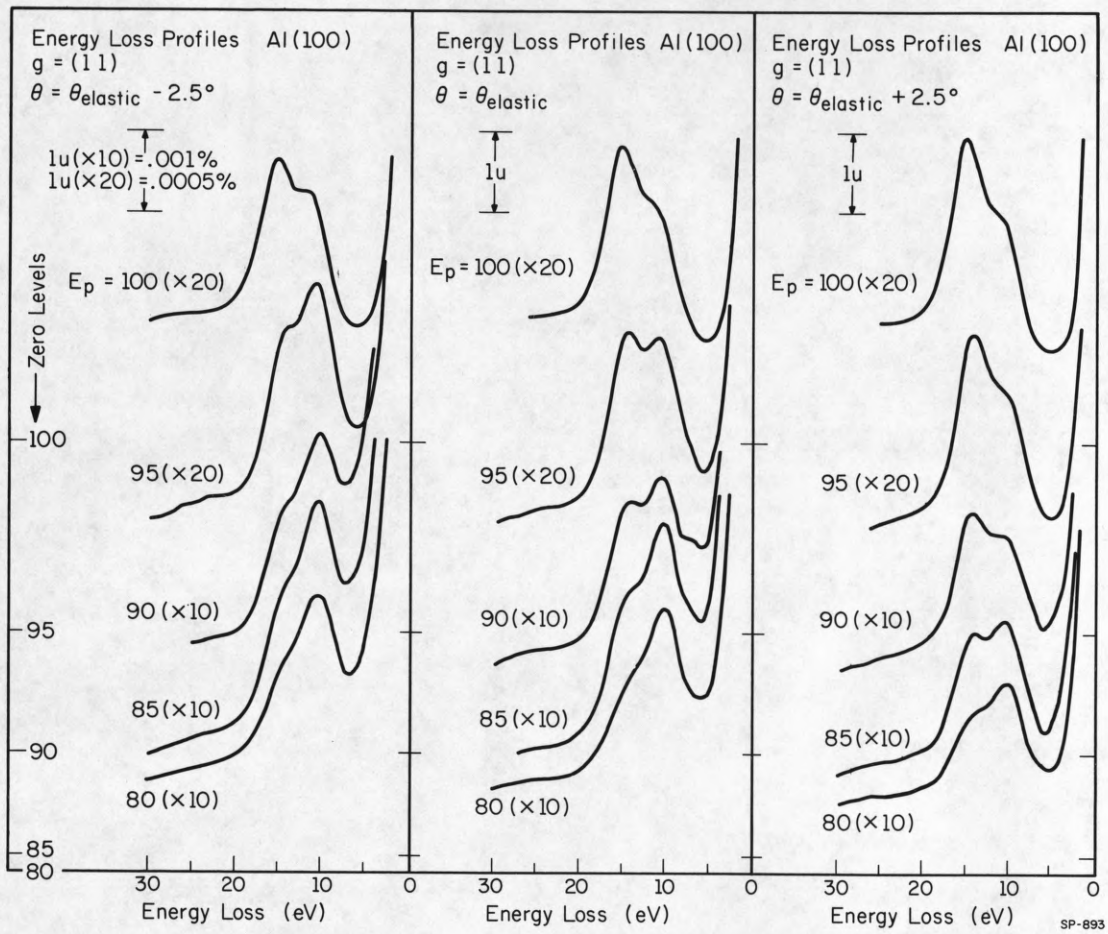

Figure 8. Series of energy loss profiles in the (11) diffraction beam for different primary energies, E_p, and collector angles θ.

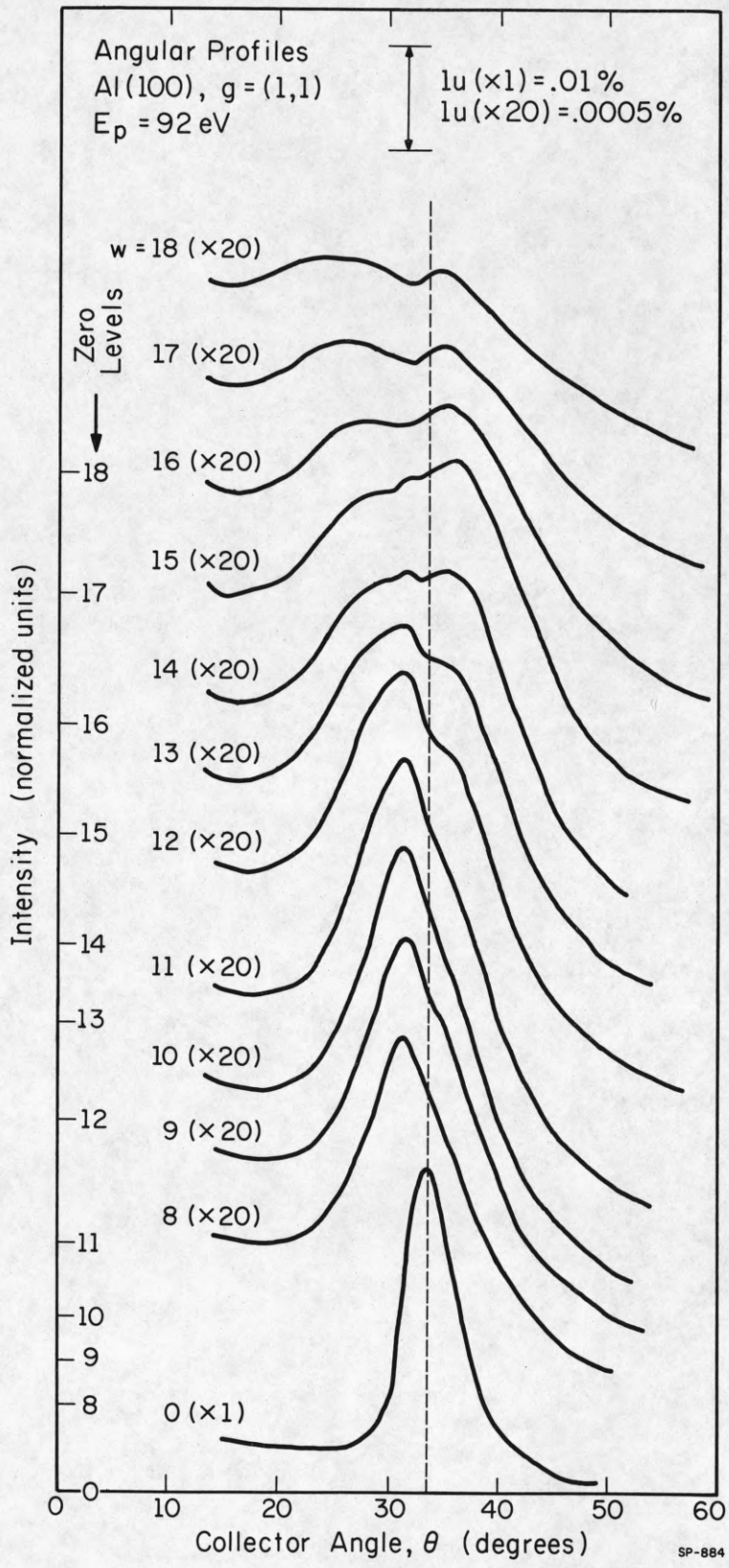

Figure 9. Angular profiles for a constant primary energy (92 eV) and different loss energies.

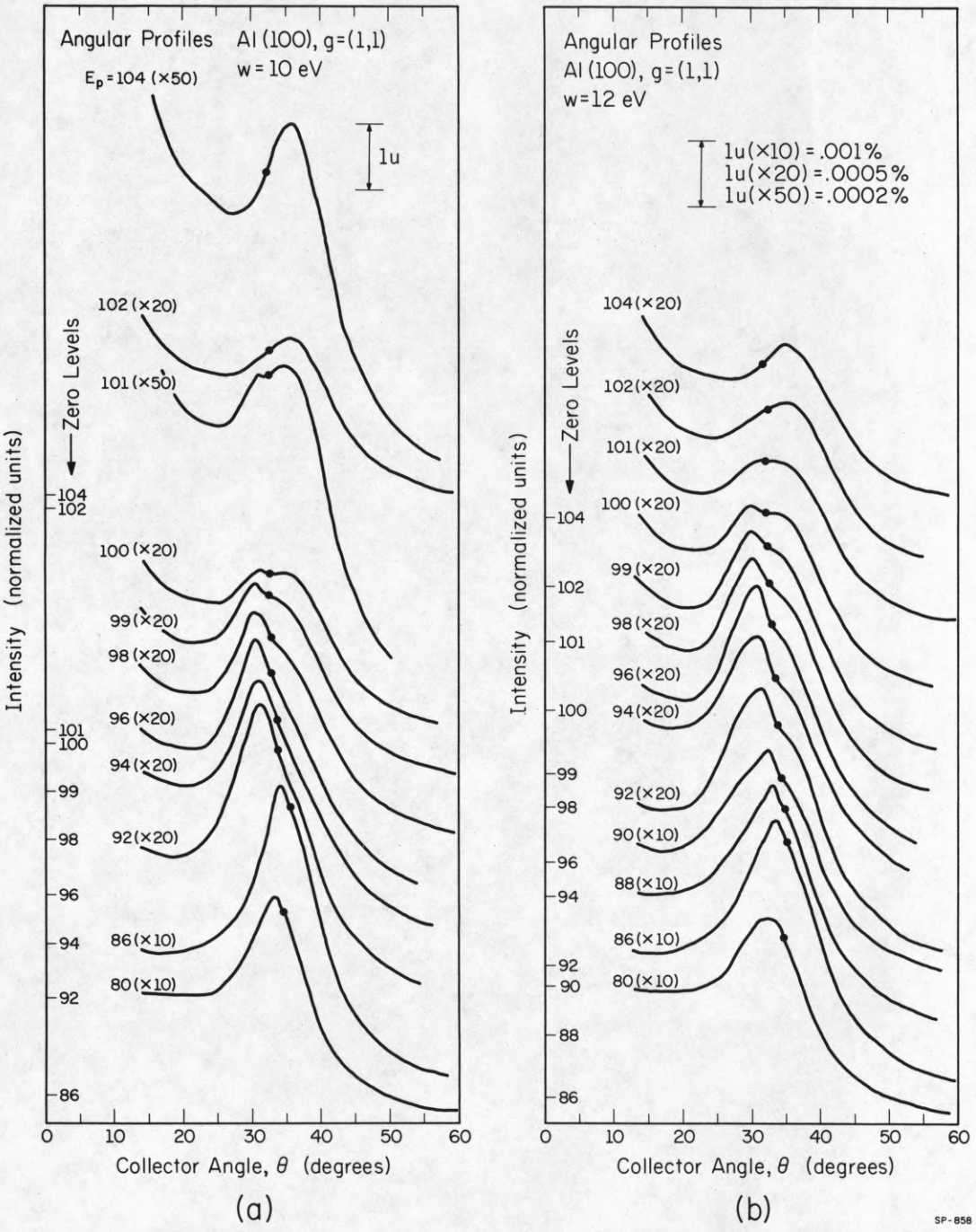

Figure 10. Inelastic angular profiles for (a) w = 10 eV, (b) w = 12 eV, in the (11) diffraction direction. Each black dot indicates the position of the peak in the elastic angular profile for that particular incident energy.

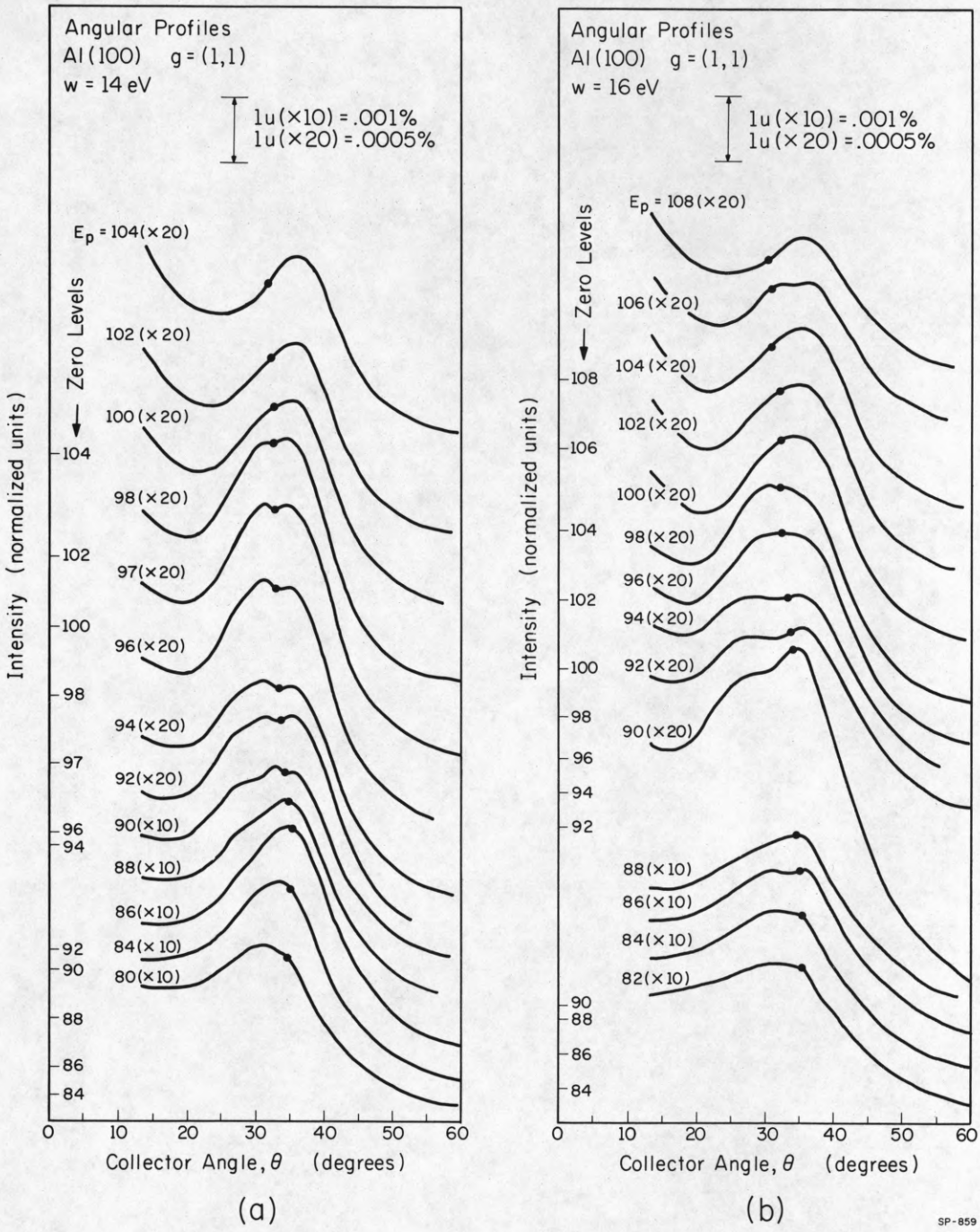

Figure 11. Inelastic angular profiles for (a) w = 14 eV, (b) w = 16 eV, in the (11) diffraction direction. Each black dot indicates the position of the peak in the elastic angular profile for that particular incident energy.

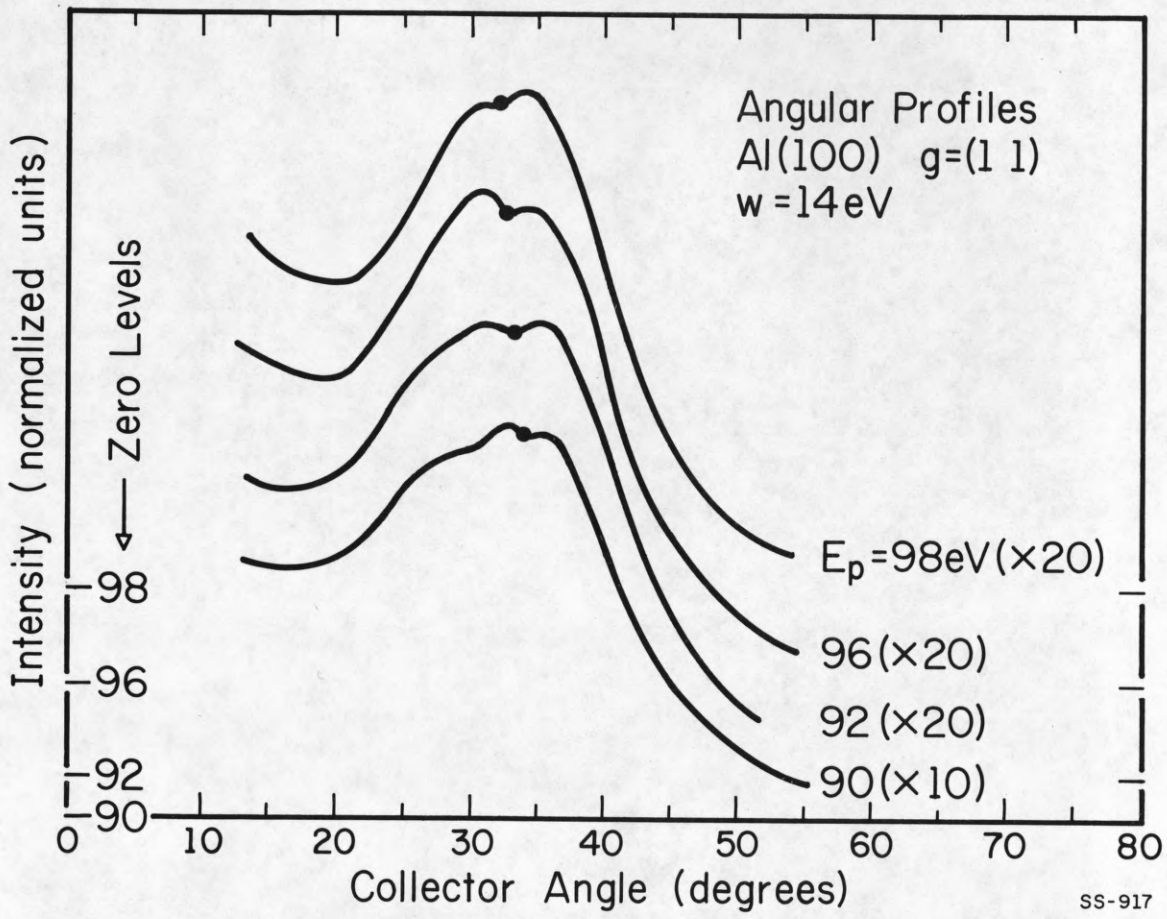

Figure 12. Inelastic angular profiles, w = 14 eV, in the (11) direction. Each black dot indicates the position of $\theta_{Elastic}$ for each primary energy.

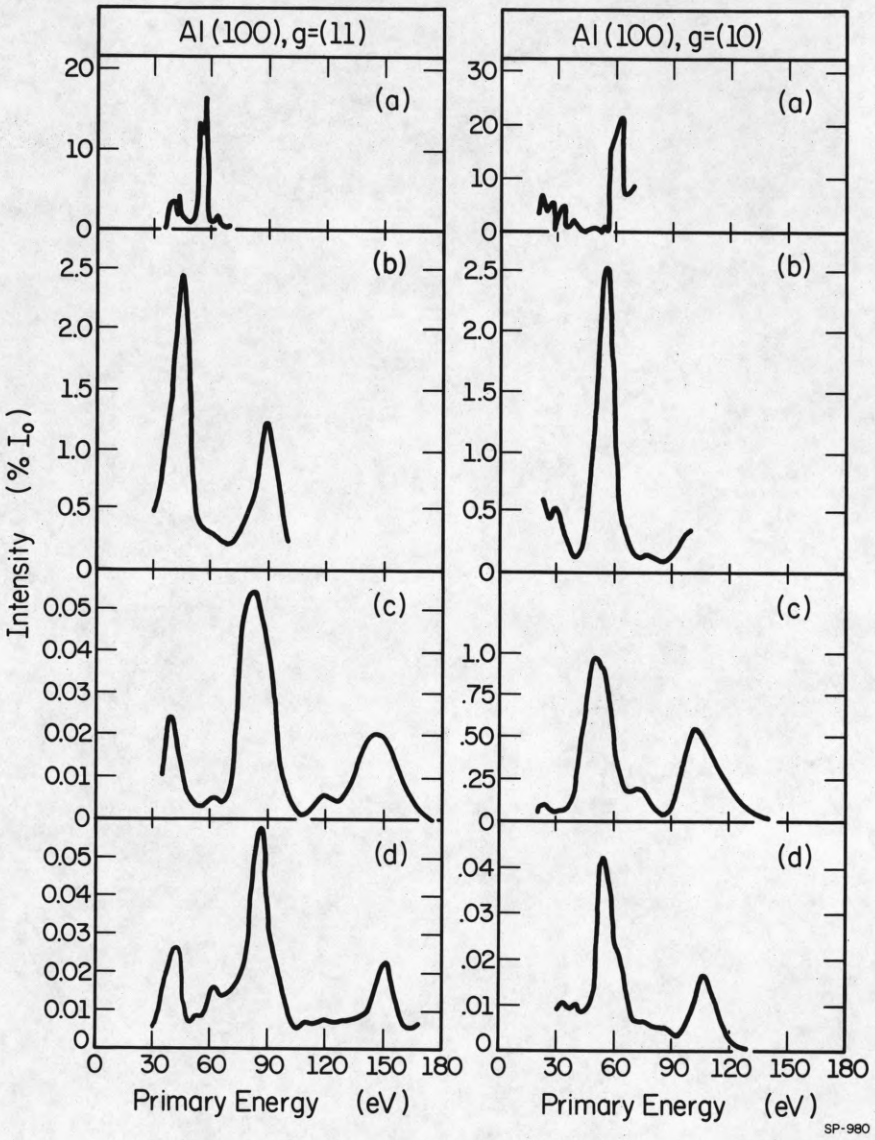

Figure 13. Theoretical, (a-c), and experimental, (d), elastic energy intensity profiles in the (11) and (10) diffraction directions. The theoretical profiles are by (a) Jepsen et al.[10], (b) Hirabayashi[11], and (c) Laramore and Duke[8].

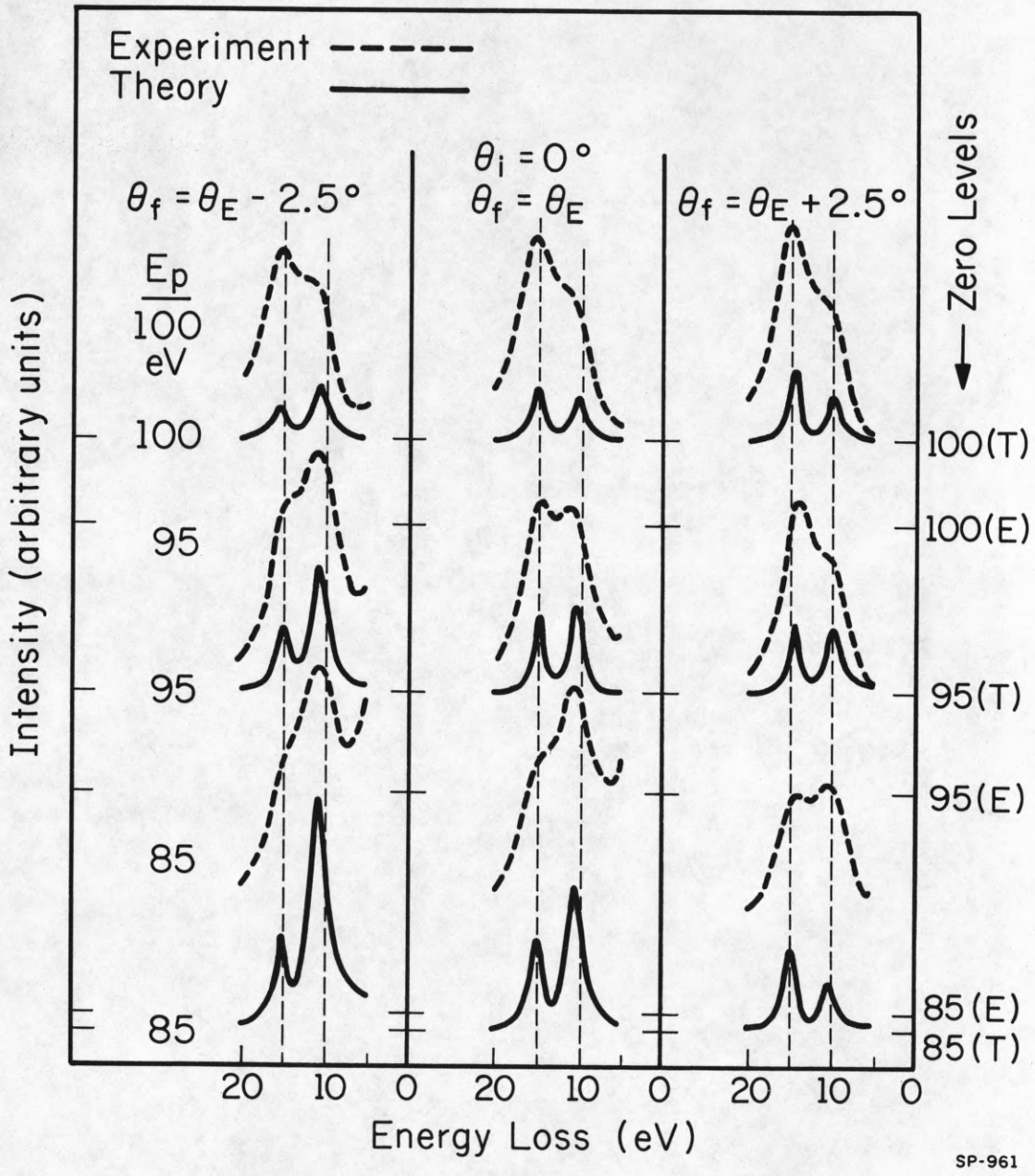

Figure 14. Theoretical and experimental energy loss profiles in the (11) diffraction direction. The theoretical profiles were calculated by Duke and Bagchi[1,3].

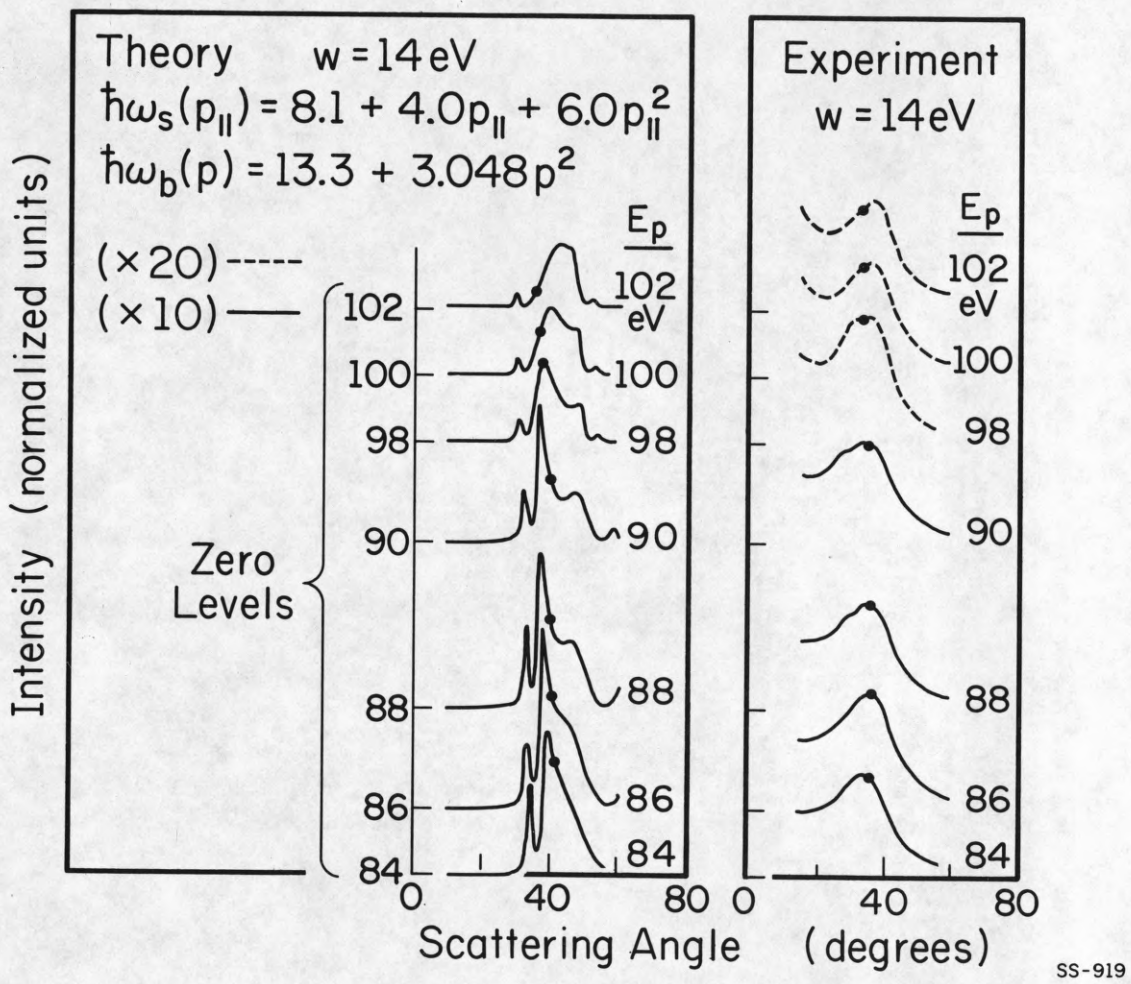

Figure 15. Theoretical and experimental inelastic angular profiles in the (11) diffraction direction for a loss energy of 14 eV. The theoretical profiles were calculated by Duke and Bagchi[1,3].

Security Classification

DOCUMENT CONTROL DATA - R & D

(Security classification of title, body of abstract and indexing annotation must be entered when the overall report is classified)

1. ORIGINATING ACTIVITY *(Corporate author)*

Coordinated Science Laboratory
University of Illinois
Urbana, Illinois 61801

2a. REPORT SECURITY CLASSIFICATION
UNCLASSIFIED

2b. GROUP

3. REPORT TITLE

ABSOLUTE INTENSITY MEASUREMENTS OF ELASTIC AND INELASTIC LOW ENERGY ELECTRON DIFFRACTION FROM Al (100)

4. DESCRIPTIVE NOTES *(Type of report and inclusive dates)*

5. AUTHOR(S) *(First name, middle initial, last name)*

James M. Burkstrand

6. REPORT DATE	7a. TOTAL NO. OF PAGES	7b. NO. OF REFS
April, 1972	49	47

8a. CONTRACT OR GRANT NO. DAAB-07-67-C-0199; PRF 3668-A3,5; AFOSR-71-2034

b. PROJECT NO.

c.

d.

9a. ORIGINATOR'S REPORT NUMBER(S)
R-555

9b. OTHER REPORT NO(S) *(Any other numbers that may be assigned this report)*
UILU-ENG 72-2216

10. DISTRIBUTION STATEMENT
This document has been approved for public release and sale; its distribution is unlimited.

11. SUPPLEMENTARY NOTES

12. SPONSORING MILITARY ACTIVITY
Joint Services Electronics Program through U. S. Army Electronics Command; Air Force Office of Scientific Research

13. ABSTRACT

Elastic and inelastic low energy electron diffraction (ELEED, ILEED) observations have been made on a clean surface of Al(100). Measurements on the (10) and (11) elastic diffractions beams were made using normally incident electrons in the energy range $30 \leq E \leq 170$ eV. Peaks in the energy loss distribution are seen near 5, 10, 15 26 and 31 eV, the dominant peaks near 10 and 15 eV corresponding to surface and bulk plasmon excitations respectively. Two types of structure are observed in the inelastic angular profiles: one closely correlated with the structure in the elastic angular profile, and the second being substructure corresponding to different ILEED conditions. Energy intensity profiles (as a function of incident energy) for the (10) and (11) elastic and inelastic diffraction beams have been measured. These profiles also show primary and secondary structure. Within the substructure of the angular and energy intensity profiles are the first experimental observations of sideband diffraction. A comparison of the experimental results and the theoretical predictions of different models is made.

DD FORM 1 NOV 65 1473

Security Classification

14. KEY WORDS	LINK A		LINK B		LINK C	
	ROLE	WT	ROLE	WT	ROLE	WT
Low energy electron diffraction (elastic and inelastic)						
Sideband diffraction						